





Doubling the superconducting transition temperature of ultraclean wafer-scale aluminum nanofilms

Ching-Chen Yeh ^{1,*} Thi-Hien Do,^{2,*} Pin-Chi Liao,¹ Chia-Hung Hsu,³ Yi-Hsin Tu,⁴ Hsin Lin,⁵ T.-R. Chang,^{4,6,7} Siang-Chi Wang,¹ Yu-Yao Gao,² Yu-Hsun Wu,² Chu-Chun Wu,² Yu An Lai,² Ivar Martin,⁸ Sheng-Di Lin ^{2,†} Christos Panagopoulos ^{9,‡} and Chi-Te Liang ^{1,10,§}

¹*Department of Physics, National Taiwan University, Taipei 106, Taiwan*

²*Institute of Electronics, National Yang Ming Chiao Tung University, Hsinchu 300, Taiwan*

³*National Synchrotron Radiation Research Center, Hsinchu 300, Taiwan*

⁴*Department of Physics, National Cheng Kung University, Tainan 701, Taiwan*

⁵*Institute of Physics, Academia Sinica, Taipei 115, Taiwan*


⁶*Center for Quantum Frontiers of Research and Technology (QFort), Tainan 701, Taiwan*

⁷*Physics Division, National Center for Theoretical Sciences, Taipei 106, Taiwan*

⁸*Materials Science Division, Argonne National Laboratory, Argonne, Illinois 08540, USA*

⁹*Division of Physics and Applied Physics, School of Physical and Mathematical Sciences, Nanyang Technological University, 21 Nanyang Link 637371, Singapore*

¹⁰*Center for Quantum Science and Engineering, National Taiwan University, Taipei 106, Taiwan*

 (Received 13 May 2023; revised 24 July 2023; accepted 11 October 2023; published 3 November 2023)

We studied the role of reduced dimensionality and disorder in the superconducting properties of wafer-scale aluminum (Al) nanofilms. This new generation of ultrathin films were grown using molecular beam epitaxy and depict normal-state sheet resistance at least 20 times lower than the quantum resistance $h/(4e^2)$. Defying general expectations, the superconducting transition temperature of our films increases with decreasing Al film thickness, reaching 2.4 K for a 3.5-nm-thick Al film grown on GaAs: twice that of bulk Al (1.2 K). Surface phonon softening is shown to impact superconductivity in pure ultrathin films, offering a route for materials engineering in two dimensions.

DOI: [10.1103/PhysRevMaterials.7.114801](https://doi.org/10.1103/PhysRevMaterials.7.114801)

I. INTRODUCTION

Superconductivity in thin films of conventional superconductors is anticipated to be suppressed with decreasing sample thickness, leading to a superconductor-insulator transition [1,2]. Early studies on aluminum (Al) however, reported unexpected enhancement of the superconducting transition temperature T_c in thin films, which were polycrystalline, granular, or included Ge or Al_2O_3 [3–9]. The apparent contrast on the effect of thickness on superconductivity [1–21] challenged our understanding of disorder-induced localization of Cooper pairs, Coulomb screening, and the generation and unbinding of vortex-antivortex pairs in low dimensions. The intrinsic trend of T_c with film thickness has remained an enigma for several decades with the discussion rekindled recently, following results on single-layer FeSe showing an unprecedentedly high T_c compared to the bulk counterpart [10–13].

Theoretically, an increase of T_c in thin films was predicted by Blatt and Thompson [22]. The basic effect relies on an enhanced electronic density of states (DOS) due to

electronic confinement. Here, each transverse electronic subband has approximately a constant density of states, with the total exceeding the bulk density of states at the Fermi level, thus enhancing T_c . The effect becomes particularly noticeable when only a small number n of transverse subbands is occupied; there the relative enhancement of DOS scales as $1/n$. Subsequent detailed calculations [23] took into account the renormalization of the chemical potential in thin films and pointed out that the strength of the confining potential matters (T_c is enhanced for strong confinement and may be suppressed for weak confinement, which points to the importance of the substrate). It was also shown that the transverse confinement of phonons leads to additional features in T_c [24]. These theoretical models provide a clear motivation for studying superconductivity in thin films and guide more detailed microscopic calculations.

To clarify the effect of film thickness on T_c , we have grown a series of pure Al ultrathin films on three different substrates using molecular beam epitaxy (MBE) and investigated both the electronic and structural properties (Supplemental Material [25]). In addition to being a well-studied conventional BCS superconductor, Al is the most abundant metallic element in the Earth's crust and employed in a plethora of applications. These include heat sinks [26], interconnects [27], plasmonics [28], superconducting detectors [29], metallic supercurrent field-effect transistors [30], and quantum

*These authors contributed equally to this work.

†sdlin@mail.nctu.edu.tw

‡christos@ntu.edu.sg

§ctliang@phys.ntu.edu.tw

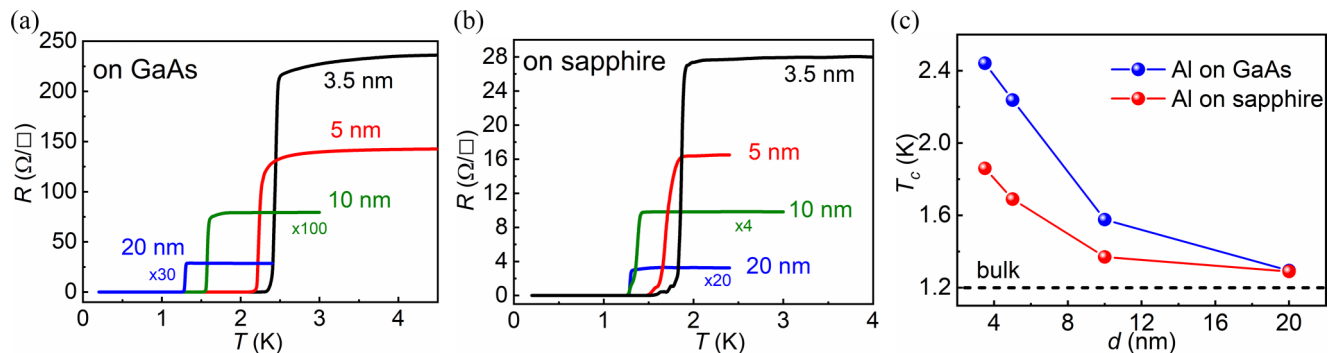


FIG. 1. Sheet resistance R as a function of temperature for (a) Al nanofilms of different thicknesses d grown on GaAs. (b) Al nanofilms of different thicknesses grown on sapphire. (c) Critical temperature T_c for Al films of different thicknesses grown on GaAs and on sapphire.

computation, science, and technology [31]. Identifying the mechanism governing T_c in wafer-scale pure nanofilms would allow one to explore superconductivity in the ultrathin film limit and to develop a recipe for quality control in the many applications of Al. Moreover, enhancing T_c in relevant nanostructures may lead to the much desired, lower quasiparticle concentration at millikelvin temperatures, substantially increasing the coherence time of a superconducting qubit [32].

II. METHODS

Ultrathin epitaxial Al films were grown in a Varian Gen-II III-V solid-source MBE system [33–35]. Si, GaAs, and sapphire substrates were pretreated prior to depositing the Al films. Before loading the substrate into the MBE chamber, the phosphorus-doped Si(111) wafer was treated as described previously [33]. All Si, GaAs, and sapphire wafers were loaded into the MBE chamber and baked at 200 °C at the exit/entry chamber for 8 h to remove moisture from the surface. Subsequently, Si and GaAs were heated to 400 °C for 5 h, while sapphire was heated to 550 °C for 5 h to remove any organic residues in the preparation chamber. In the growth chamber, the Si wafer was heated to 630 °C and cooled in the ultrahigh-vacuum chamber to less than 0 °C before the Al nanofilm was deposited. Prior to depositing Al, a semi-insulating GaAs(001) substrate was heated to 600 °C for 20 min to remove the native oxide, and a 200-nm-thick undoped GaAs buffer layer was then grown at 580 °C. Following that, the GaAs substrate was heated for 3 min to 600 °C without As flux to develop a Ga-rich surface. The GaAs wafer was subsequently cooled in the ultrahigh-vacuum chamber to less than 0 °C. The Al nanofilm was deposited after the residual As in the growth chamber was pumped out in a background pressure below 2×10^{-10} Torr. The sapphire (0001) substrate was heated to 650 °C for 1 h to remove the native oxide, and then cooled to less than 0 °C. The Al nanofilm was subsequently grown on the treated sapphire substrate. All the measured Al samples were cut near the center of the respective MBE-grown wafers.

III. RESULTS

A. Electrical measurements

Figures 1(a) and 1(b) depict the sheet resistance R for Al films of different thicknesses grown on GaAs and on sapphire,

respectively. T_c is the temperature at which the resistance ratio crosses 50% of R/R_N . Plots of the ratio of sheet resistance to the normal-state sheet resistance as a function of temperature $R/R_N(T)$ are shown in the Supplemental Material [25], Fig. S1. T_c decreases with increasing film thickness d [Fig. 1(c)]. For Al films in the range $3.5 \text{ nm} \leq d \leq 10 \text{ nm}$, T_c is higher for films grown on GaAs and converges to the value for bulk Al (1.2 K) for thicker films ($d = 20 \text{ nm}$) [Fig. 1(c)]. Notably, our results are not inconsistent with those reported [1,2] since our samples are much less resistive [at least 20 times lower than $h/(4e^2)$] compared to those showing the superconductor-insulator transition with decreasing the film thickness.

To further probe the observed enhanced superconductivity in the 3.5-nm-thick Al films grown on GaAs and sapphire, we performed electrical measurements on these two sets of films, as well as a counterpart film grown on Si (Supplemental Material [25], Fig. S1). The high quality of our Al nanofilms is further reflected in the slight differences between the transition temperatures determined from $R = 0.9R_N$ and $R = 0.1R_N$ (Supplemental Material [25], Fig. S2). Moreover, the 3.5-nm-thick Al films grown on the 2-in. GaAs, 3-in. sapphire, and 2-in. Si substrates all show high uniformity across the wafers (Supplemental Material [25], Fig. S3).

Using out-of-plane magneto-sheet resistance data $R^\perp(H)$ obtained on 3.5-nm-thick Al films at different temperatures (Supplemental Material [25], Fig. S4), we identify H_{c2} as the magnetic field where R^\perp crosses 50% of its residual normal-state value. The measured H_{c2} 's are all enhanced over the bulk critical field value (10 mT).

B. Structural studies

Next, we discuss the structural properties of our samples. Atomic force microscopy on 3.5-nm-thick Al films reveals rms roughness of 0.265, 0.268, and 0.316 nm for Al nanofilms grown on GaAs, sapphire, and Si, respectively (Supplemental Material [25], Fig. S5). X-ray diffraction (XRD) 2θ - θ scans along the surface normal, in units of substrate reciprocal lattice unit depict weak and broad albeit pronounced Al(111) peaks for films grown on Si and sapphire substrates [Figs. 2(b) and 2(c)], whereas for films grown on GaAs, we observed a weaker and broader Al(111) peak on a strong background [Fig. 2(a)]. The broad peak widths are ascribed mainly to the small film thickness.

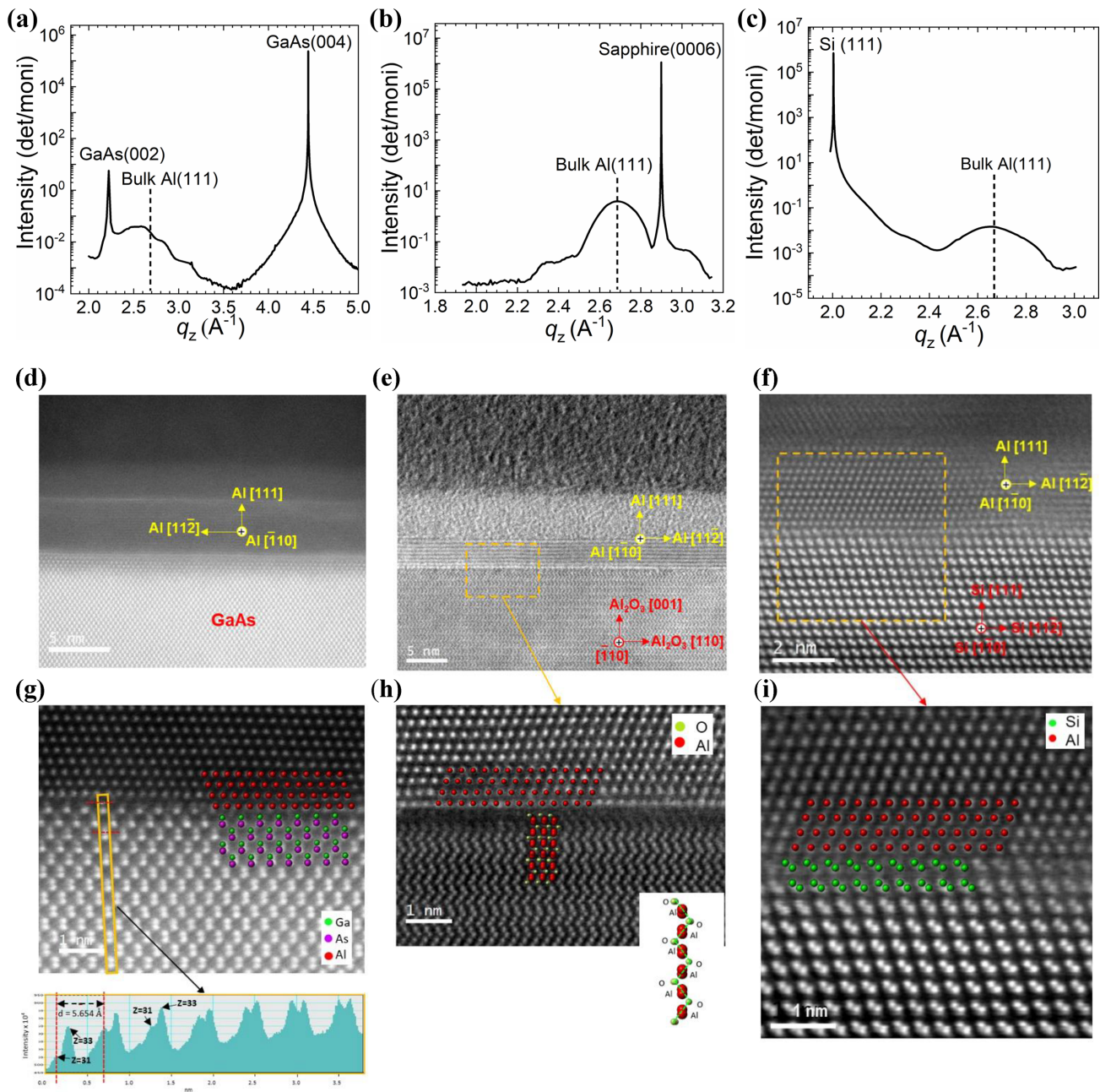


FIG. 2. XRD radial scans along surface normal of 3.5-nm-thick Al films grown on (a) GaAs, (b) sapphire, and (c) Si, respectively. The corresponding q_z 's for bulk Al(111) are indicated by the dotted lines. (d)–(f) Top panel: Cross-sectional HAADF images of 3.5-nm-thick Al films grown (d) on GaAs, (e) on sapphire, and (f) on Si, respectively. (g)–(i) Enlarged selected areas of 3.5-nm-thick Al films.

We also performed lateral radial scans for Al films grown on GaAs, sapphire, and Si substrates (Supplemental Material [25], Fig. S6). For 3.5-nm-thick films on sapphire and Si, the Al($2\bar{2}0$) reflection exhibits a lattice constant close to bulk Al. There is also a peak (peak B) in addition to the Al($2\bar{2}0$) reflection (peak A) in the lateral radial scan along [110] in GaAs. Furthermore, the corresponding interplanar spacing (1.43 \AA) of peak A agrees with that of the bulk Al($2\bar{2}0$) reflection. Analysis shows peak B has a different structure from peak A and is associated with the region nearer the surface (Supplemental Material [25], Fig. S7). All XRD results indicate our Al(111) films were grown epitaxially on GaAs(001), *c*-plane (0001) sapphire, and Si(111) substrates.

Microstructure studies using high-resolution scanning transmission electron microscopy (STEM) add credence to the epitaxial growth of our Al films. Figures 2(d)–2(f) depict cross-sectional high-angle annular dark field (HAADF) images revealing high-quality ultrathin epitaxial Al films on GaAs, sapphire, and Si. Corresponding fast-Fourier-transform patterns (not shown) indicate an orientation consistent with the above-mentioned XRD results. Furthermore, the interfaces are sharp with no interlayer mixing between Al films and substrates.

Using enlarged atomic-resolution HAADF images of the selected area in Figs. 2(h) and 2(i), we resolved the atomic structure of Al films and substrates, revealing interfacial

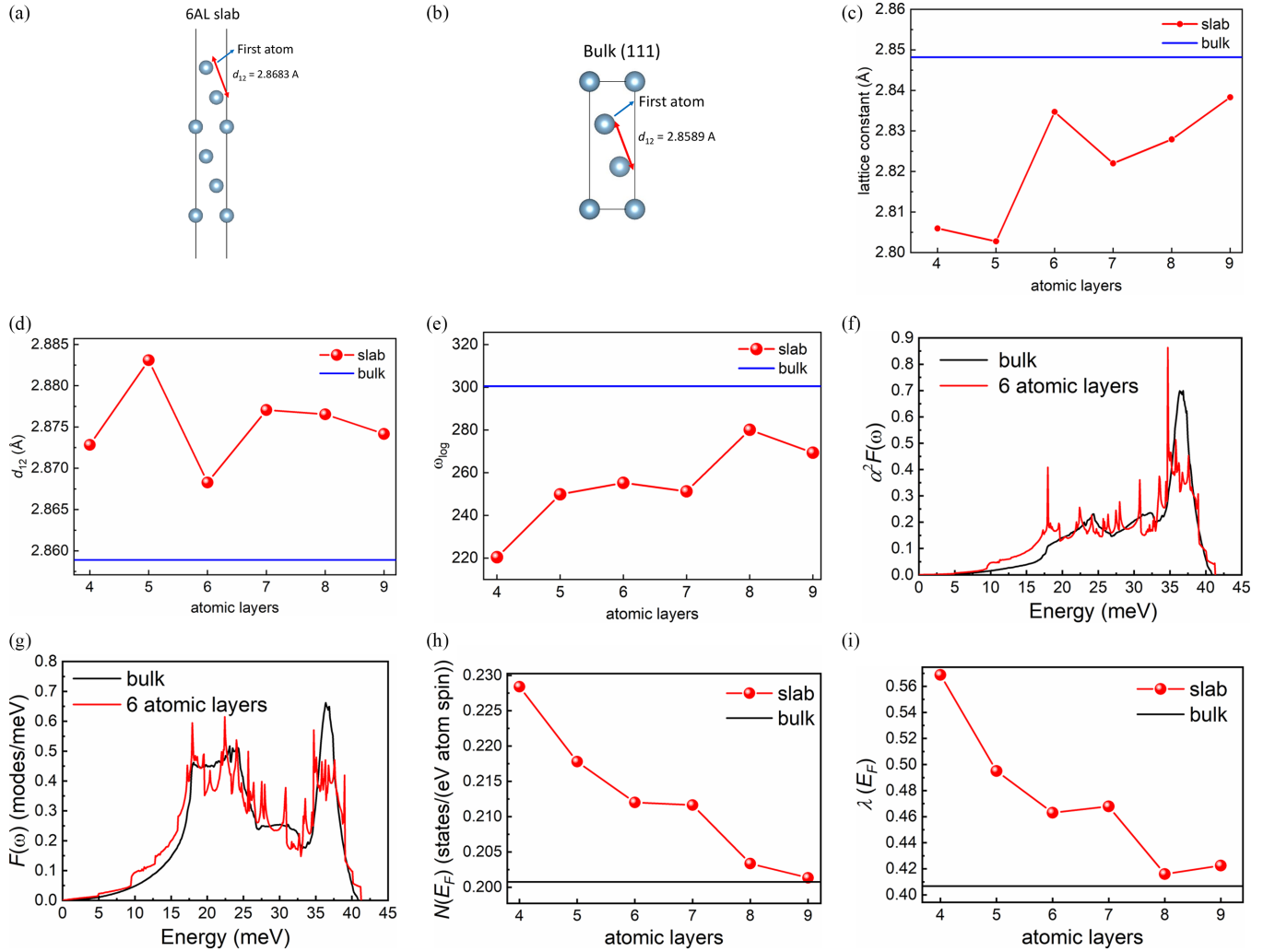


FIG. 3. (a) and (b) Models for performing substrate-free DFT calculations. Thickness dependence of (c) the lattice constant, (d) the distance between the first and second atom from the topmost surface d_{12} , and (e) ω_{\log} . We note that the d_{12} profile is not monotonic because the lattice constant varies as well. Notably, d_{12} for all thin films is larger than that in bulk Al. (f) Isotropic Eliashberg spectral function $\alpha^2 F(\omega)$. (g) Phonon density of states $F(\omega)$. For comparison, the curves are normalized such that $\int F(\omega) d\omega = 9$. (h) Thickness dependence of $N(E_F)$. (i) Thickness dependence of λ .

bonding of Al-O and Al-Si for the Al films grown on sapphire and Si substrates, respectively. The enlarged image of Fig. 3(g) depicts the Al/GaAs interface and dumbbell structure of Ga/As atomic columns. We note, $Z_{\text{Ga}} = 31$ and $Z_{\text{As}} = 33$. We verified the Ga/As atomic columns, using the STEM intensity profile across the dumbbell. As shown in the inset of Fig. 2(g), both Ga and As atomic columns can be resolved. The terminating plane is Ga, in agreement with the surface treatment condition before growth (Ga-rich surface). Hence, the interfacial bonding is Al-Ga.

C. Density functional theory calculations

Having characterized the structural and electronic properties of our Al films, we turn our attention to the physical mechanism leading to the enhancement of T_c with decreasing film thickness. Density functional theory (DFT) calculations were performed with the QUANTUM ESPRESSO package [36,37] using norm-conserving scalar-relativistic pseudopotentials

[38] within the generalized gradient approximation–Perdew–Burke–Ernzerhof approximation [39] and a plane-wave cutoff of 80 Ry. The \mathbf{k} mesh of $12 \times 12 \times 6$ and $12 \times 12 \times 1$ is used for bulk and thin films, respectively. The structure was fully relaxed until the remanent forces were less than $0.136 \text{ meV}/\text{\AA}$. The electron-phonon calculations were computed within density functional perturbation theory [40] on the $6 \times 6 \times 3$ and $6 \times 6 \times 1$ \mathbf{q} mesh for bulk and thin films, respectively. The electron-phonon coupling strength λ is given by

$$\lambda = \sum_{\mathbf{q}\nu} \lambda_{\mathbf{q}\nu} = \sum_{\mathbf{q}\nu} \frac{1}{\pi N(E_F)} \frac{\gamma_{\mathbf{q}\nu}}{\omega_{\mathbf{q}\nu}^2} = 2 \int \frac{\alpha^2 F(\omega)}{\omega} d\omega, \quad (1)$$

where

$$\alpha^2 F(\omega) = \frac{1}{2\pi N(E_F)} \sum_{\mathbf{q}\nu} \frac{\gamma_{\mathbf{q}\nu}}{\omega_{\mathbf{q}\nu}} \delta(\omega - \omega_{\mathbf{q}\nu}) \quad (2)$$

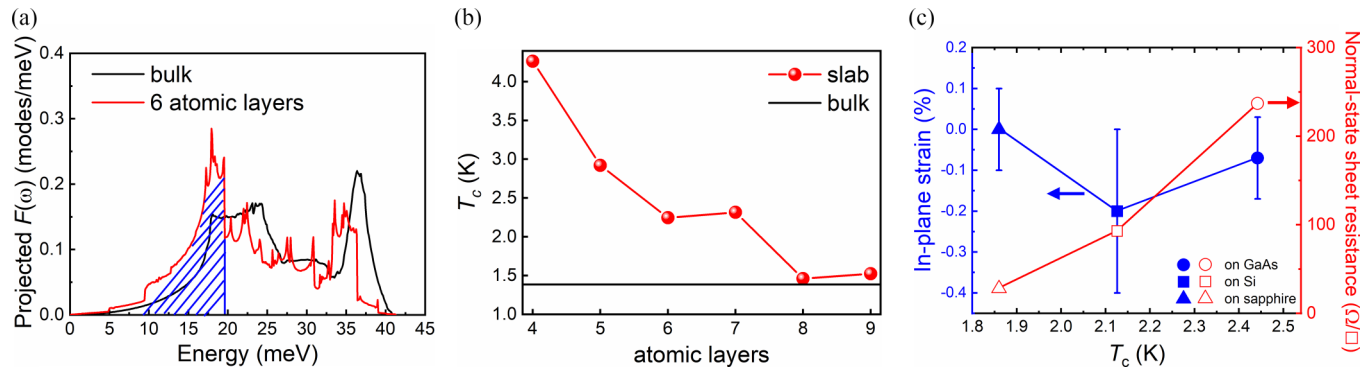


FIG. 4. (a) Projected phonon density of states for the topmost surface atom. The black and red curves correspond to bulk and six-layer Al thin film, respectively. The hatched regions indicate phonon softening in thin Al films in the low-energy regime. (b) Thickness dependence of T_c . (c) T_c versus in-plane strain and low- T normal-state sheet resistance for the 3.5-nm-thick Al films on the three different substrates explored in this study. The highest normal-state sheet resistance in our films is 20 times lower than the quantum resistance $h/(4e^2)$.

is the isotropic Eliashberg spectral function, ν is the index of phonon modes, $N(E_F)$ is the electronic DOS at the Fermi level, and $\gamma_{\mathbf{q}\nu}$ are phonon linewidths. We note that the phonon linewidths themselves are proportional to the electronic density of states; therefore (1) and (2), despite the appearances, increase with $N(E_F)$. From Fig. 3(h), $N(E_F)$ increases with the decreasing thickness. This is indeed expected in the limit of strong confinement [23]. Thus, the theoretical enhancement of T_c can be attributed both to the phonon softening and to the increased phonon DOS as well as an increase in the electronic DOS. The critical temperature T_c was estimated by the McMillan equation in the Allen-Dynes form [41,42]:

$$T_c = \frac{\omega_{\log}}{1.2} \exp \left[-\frac{1.04(1 + \lambda)}{\lambda - \mu^*(1 + 0.62\lambda)} \right], \quad (3)$$

where

$$\omega_{\log} = \exp \left[\frac{2}{\lambda} \int \ln(\omega) \frac{\alpha^2 F(\omega)}{\omega} d\omega \right] \quad (4)$$

is the logarithmic average frequency [Fig. 3(e)]. The parameter μ^* is chosen to be 0.1.

We determined the electronic structure, phonon DOS, and electron-phonon coupling properties via first-principles calculations [Figs. 3(a)–3(i)]. We show the isotropic Eliashberg spectral function $\alpha^2 F(\omega)$ for bulk Al and a six-layer Al thin film [Fig. 3(f)]. Compared to bulk Al, the highest frequency peak (36.5 meV) is suppressed and the intensity in the lower-energy state is increased in the six-layer Al thin film. As a result, the electron-phonon coupling strength $\lambda = 2 \int \alpha^2 F(\omega) \omega^{-1} d\omega$ increased by about 13%. The phonon DOS $F(\omega)$ exhibits a similar form to $\alpha^2 F(\omega)$ [Fig. 3(f)]. Since $\alpha^2 F(\omega)$ is related to $F(\omega)$, we can infer the trend of $\alpha^2 F(\omega)$ by studying $F(\omega)$ [Fig. 3(g)]. Based on layer-resolved decomposition, we attribute the low-energy phonon DOS mainly to surface phonons [hatched regions in Figs. 3(g) and 4(a)]. Our DFT calculations show that the spacing of Al atoms on the film surface is slightly higher than that for bulk Al [Fig. 3(d)]. This modulation will soften the surface phonon mode and increase the intensity of the low-energy phonon DOS.

The calculated electronic density of states $N(E_F)$ as a function of Al layer thickness is depicted in Fig. 3(h). Both λ and T_c increase with decreasing film thickness [Figs. 3(i)

and 4(b)], consistent with our experimental results [Fig. 1(c)]. Furthermore, Fig. 4(c) shows that T_c increases with increasing normal-state sheet resistance, in contrast to earlier studies [1,2]. Hence, the normal-state sheet resistance is not the dominant factor determining T_c for the thinnest films. Similarly, in-plane strain does not appear to govern the trend observed in T_c for the 3.5-nm-thick Al nanofilms grown on GaAs, sapphire, and Si [Fig. 4(c)]. Neither do disorder [determined by the low-temperature normal-state sheet resistance and the residual-resistance ratio $R_{300\text{ K}}/R_N$ of the three 3.5-nm-thick Al films (Supplemental Material [25], Fig. S8) and twin structures [seen as alternating peak strengths in a thick film grown on Si, and the pronounced six peaks in thick films on sapphire and on GaAs (Supplemental Material [25], Fig. S9)], or strain (Supplemental Material [25], Table S1).

D. Possible mechanisms leading to enhanced T_c

We conclude the increase in T_c is due to enhanced surface phonon softening and increased electronic density of states with decreasing film thickness. Our experimental results are in line with the work by Blatt and Thompson [22] where an enhanced electronic density of states due to confinement leads to an increase in T_c . We also note that for the 3.5-nm-thick Al films, sapphire has the largest bandgap (10.0 eV) amongst the studied substrates, yet the enhanced T_c is the lowest compared to counterparts grown on Si and GaAs.

Next, we comment on the progressive increase in T_c for the 3.5-nm-thick Al films grown on sapphire, Si, and GaAs, respectively. Earlier works (Supplemental Material [25], Fig. S10) suggest the phonon DOS for GaAs is highest in the low-frequency limit but low and broad for sapphire [43–45]. Since $\lambda \sim \alpha^2 F(\omega)/\omega$, assuming the electronic contribution from Al and the electron-phonon coupling from the substrates are similar, the low-frequency end of the phonon DOS may contribute to the rise in λ and T_c with decreasing film thickness, resulting in the observed trend in T_c for the 3.5-nm-thick Al grown on different substrates.

Compared to earlier studies [46] the low-temperature resistivities ρ of our Al films (including previous work done by some of the authors [34,35]) are significantly lower (for the relevant film thickness; Supplemental Material [25], Fig.

S11). Namely, for the 3.5-nm-thick and 5-nm-thick Al films grown on GaAs, our values for ρ are closer to Ref. [9], and lower than in Refs. [3,9], and [46] for the rest of our Al films. Also, the sheet resistances of our films are always lower than in much earlier reports (Supplemental Material [25], Fig. S11). Moreover, the scaling $d \times T_c = AR^{-B}$, does not hold for our films (Supplemental Material [25], Fig. S11(c)) [47]. These separate findings correlate the primary impact of the substrate and interface on the superconducting properties of Al epitaxial ultrathin films, calling for further investigation of this aspect.

Finally, we discuss recent *in situ* scanning tunneling microscopy studies of ultraclean Al films grown on Si(111) [21]. In this work, a threefold enhanced T_c (3.3 ± 0.1 K) was reported. The authors excluded surface oxidation as a cause for the enhanced T_c in their *in situ* study. In our work, the presence of a thin overlying AlO_x layer when the Al film is exposed to air during *ex situ* processing does not hinder the enhanced superconductivity. Moreover, Si intermixing and Si doping cannot be the origins of the enhanced T_c in the work of van Weerdenburg *et al.* [21]. Hence, enhanced superconductivity is an intrinsic property of ultrathin Al films, provided the normal-state square resistance is much lower than the quantum resistance $h/(4e^2)$. The fact that the normal-state square resistances of all our devices are at least 20 times less than $h/(4e^2)$ ensures all our devices are away from the insulator-superconductor transition.

IV. CONCLUSIONS

In summary, we report extensive transport and structural studies on high-quality wafer-scale epitaxial Al nanofilms grown by MBE. T_c increases with decreasing film thickness, in contrast to earlier studies on Bi, Pb, and Al grown on cold substrates (20 K) [1,33], Pb [48], and Nb [49]. DFT calculations suggest the observed increase in T_c is due to surface phonon

softening and enhanced electronic density of states with decreasing film thickness. Furthermore, T_c for the thinnest Al nanofilms (3.5 nm) increases when grown on sapphire, Si, and GaAs; substrates commonly employed in plasmonics, Si-based quantum computation and information and Si complementary metal-oxide semiconductor technology, and high-frequency devices, respectively. Phonon softening and enhanced electronic density of states may also increase T_c of other elemental BCS superconducting ultrathin films with normal-state square resistance lower than the quantum resistance $h/(4e^2)$, whereas a suitable choice of substrates may allow for further enhancement of T_c . Our results impact not only the long-standing investigation of superconductivity in the very thin limit but also the optimization of the normal and superconducting state properties in low-temperature technology.

ACKNOWLEDGMENTS

C.P. acknowledges support from the National Research Foundation (NRF) Singapore Competitive Research Program under Grant No. NRF-CRP21-2018-0001 and the Singapore Ministry of Education (MOE) Academic Research Fund Tier 3 under Grant No. MOE2018-T3-1-002. The work of I.M. was funded by the Materials Sciences and Engineering Division, Basic Energy Sciences, Office of Science, U.S. DOE. T.-R.C. was supported by the 2030 Cross-Generation Young Scholars Program from the National Science and Technology Council (NSTC) in Taiwan (Program No. MOST111-2628-M-006-003-MY3), National Cheng Kung University (NCKU), Taiwan, and National Center for Theoretical Sciences, Taiwan. This research was supported, in part, by Higher Education Sprout Project, Ministry of Education to the Headquarters of University Advancement at NCKU. C.-T.L., S.-D.L. and H.L. acknowledge support from the NSTC, Taiwan.

-
- [1] D. B. Haviland, Y. Liu, and A. M. Goldman, *Phys. Rev. Lett.* **62**, 2180 (1989).
 - [2] A. Yazdani and A. Kapitulnik, *Phys. Rev. Lett.* **74**, 3037 (1995).
 - [3] R. W. Cohen and B. Abeles, *Phys. Rev.* **168**, 444 (1968).
 - [4] J. J. Hauser, *Phys. Rev. B* **3**, 1611 (1971).
 - [5] R. B. Pettit and J. Silcox, *Phys. Rev. B* **13**, 2865 (1976).
 - [6] V. N. Smolyaninova, K. Zander, T. Gresock, C. Jensen, J. C. Prestigiacomo, M. S. Osofsky, and I. I. Smolyaninov, *Sci. Rep.* **5**, 15777 (2015).
 - [7] V. N. Smolyaninova, C. Jensen, W. Zimmerman, J. C. Prestigiacomo, M. S. Osofsky, H. Kim, N. Bassim, Z. Xing, M. M. Qazilbash, and I. I. Smolyaninov, *Sci. Rep.* **6**, 34140 (2016).
 - [8] L. Grünhaupt, N. Maleeva, S. T. Skacel, M. Calvo, F. Levy-Bertrand, A. V. Ustinov, H. Rotzinger, A. Monfardini, G. Catelani, and I. M. Pop, *Phys. Rev. Lett.* **121**, 117001 (2018).
 - [9] M. Strongin, R. S. Thompson, O. F. Kammerer, and J. E. Crow, *Phys. Rev. B* **1**, 1078 (1970).
 - [10] D. Liu, W. Zhang, D. Mou, J. He, Y.-B. Ou, Q.-Y. Wang, Z. Li, L. Wang, L. Zhao, S. He *et al.*, *Nat. Commun.* **3**, 931 (2012).
 - [11] J. J. Lee, F. T. Schmitt, R. G. Moore, S. Johnston, Y.-T. Cui, W. Li, M. Yi, Z. K. Liu, M. Hashimoto, Y. Zhang *et al.*, *Nature (London)* **515**, 245 (2014).
 - [12] J.-F. Ge, Z.-L. Liu, C. Liu, C.-L. Gao, D. Qian, Q.-K. Xue, Y. Liu, and J.-F. Jia, *Nat. Mater.* **14**, 285 (2015).
 - [13] H. Ding, Y.-F. Lv, K. Zhao, W.-L. Wang, L. Wang, C.-L. Song, X. Chen, X.-C. Ma, and Q.-K. Xue, *Phys. Rev. Lett.* **117**, 067001 (2016).
 - [14] H.-M. Zhang, Y. Sun, W. Li, J.-P. Peng, C.-L. Song, Y. Xing, Q. Zhang, J. Guan, Z. Li, Y. Zhao *et al.*, *Phys. Rev. Lett.* **114**, 107003 (2015).
 - [15] C. Zhang, F. Hao, G. Gao, X. Liu, C. Ma, Y. Lin, Y. Yin, and X. Li, *npj Quantum Mater.* **2**, 2 (2017).
 - [16] D. A. Rhodes, A. Jindal, N. F. Q. Yuan, Y. Jung, A. Antony, H. Wang, B. Kim, Y.-C. Chiu, T. Taniguchi, K. Watanabe *et al.*, *Nano Lett.* **21**, 2505 (2021).
 - [17] E. Khestanova, J. Birkbeck, M. Zhu, Y. Cao, G. L. Yu, D. Ghazaryan, J. Yin, H. Berger, L. Forró, T. Taniguchi *et al.*, *Nano Lett.* **18**, 2623 (2018).

- [18] S. Mandal, S. Dutta, S. Basistha, I. Roy, J. Jesudasan, V. Bagwe, L. Benfatto, A. Thamizhavel, and P. Raychaudhuri, *Phys. Rev. B* **102**, 060501(R) (2020).
- [19] S. Giaremis, Ph. Komninou, Th. Karakostas, and J. Kioseoglou, *J. Low Temp. Phys.* **203**, 180 (2021).
- [20] A. A. Shanenko, M. D. Croitoru, and F. M. Peeters, *Europhys. Lett.* **76**, 498 (2006).
- [21] W. van Weerdenburg, A. Kamlapure, E. Holm Fyhn, X. Huang, N. P. E. van Mullekom, M. Steinbrecher, P. Krogstrup, J. Linder, and A. A. Khajetoorians, *Sci. Adv.* **9**, eadf5500 (2023).
- [22] J. M. Blatt and C. J. Thompson, *Phys. Rev. Lett.* **10**, 332 (1963).
- [23] D. Valentinis, D. van der Marel, and C. Berthod, *Phys. Rev. B* **94**, 054516 (2016).
- [24] E. H. Hwang, S. Das Sarma, and M. A. Stroschio, *Phys. Rev. B* **61**, 8659 (2000).
- [25] See Supplemental Material at <http://link.aps.org/supplemental/10.1103/PhysRevMaterials.7.114801> for more details.
- [26] M. Shaukatullah, W. R. Storr, B. J. Hansen, and M. A. Gaynes, *IEEE Trans. Compon. Packag. Manuf. Technol. Part A* **19**, 486 (1996).
- [27] H. Niwa, H. Yagi, and H. Tsuchikawa, *J. Appl. Phys.* **68**, 328 (1990).
- [28] M. W. Knight, N. S. King, L. Liu, H. O. Everitt, P. Nordlander, and N. J. Halas, *ACS Nano* **8**, 834 (2014).
- [29] P. K. Day, H. G. LeDuc, B. A. Mazin, A. Vayonakis, and J. Zmuidzinas, *Nature (London)* **425**, 817 (2003).
- [30] G. De Simoni, F. Paolucci, P. Solinas, E. Strambini, and F. Giazotto, *Nat. Nanotechnol.* **13**, 802 (2018).
- [31] L. Grünhaupt, M. Spiecker, D. Gusenkova, N. Maleeva, S. T. Skacel, I. Takmakov, F. Valenti, P. Winkel, H. Rotzinger, W. Wernsdorfer *et al.*, *Nat. Mater.* **18**, 816 (2019).
- [32] S. Gustavsson, F. Yan, G. Catelani, J. Bylander, A. Kamal, J. Birenbaum, D. Hover, D. Rosenberg, G. Samach, A. P. Sears *et al.*, *Science* **354**, 1573 (2016).
- [33] Y. H. Tsai, Y.-H. Wu, Y.-Y. Ting, C.-C. Wu, J.-S. Wu, and S.-D. Lin, *AIP Adv.* **9**, 105001 (2019).
- [34] Y.-T. Fan, M.-C. Lo, C.-C. Wu, P.-Y. Chen, J.-S. Wu, C.-T. Liang, and S.-D. Lin, *AIP Adv.* **7**, 075213 (2017).
- [35] A. Kumar, G.-M. Su, C.-S. Chang, C.-C. Yeh, B.-Y. Wu, D. K. Patel, Y.-T. Fan, S.-D. Lin, L. Chow, and Chi-Te Liang, *J. Nanomater.* **2019**, 6376529 (2019).
- [36] P. Giannozzi, S. Baroni, N. Bonini, M. Calandra, R. Car, C. Cavazzoni, D. Ceresoli, G. L. Chiarotti, M. Cococcioni, I. Dabo *et al.*, *J. Phys.: Condens. Matter* **21**, 395502 (2009).
- [37] P. Giannozzi, O. Andreussi, T. Brumme, O. Bunau, M. B. Nardelli, M. Calandra, R. Car, C. Cavazzoni, D. Ceresoli, M. Cococcioni *et al.*, *J. Phys.: Condens. Matter* **29**, 465901 (2017).
- [38] D. R. Hamann, *Phys. Rev. B* **88**, 085117 (2013).
- [39] J. P. Perdew, K. Burke, and M. Ernzerhof, *Phys. Rev. Lett.* **77**, 3865 (1996).
- [40] S. Baroni, S. de Gironcoli, A. Dal Corso, and P. Giannozzi, *Rev. Mod. Phys.* **73**, 515 (2001).
- [41] W. L. McMillan, *Phys. Rev.* **167**, 331 (1968).
- [42] P. B. Allen and R. C. Dynes, *Phys. Rev. B* **12**, 905 (1975).
- [43] https://docs.quantumatk.com/tutorials/phonon_bs/phonon_bs.html.
- [44] Z. Cheng, Y. R. Koh, H. Ahmad, R. Hu, J. Shi, M. E. Liao, Y. Wang, T. Bai, R. Li, E. Lee *et al.*, *Commun. Phys.* **3**, 115 (2020).
- [45] J. E. Herriman and B. Fultz, *Phys. Rev. B* **101**, 214108 (2020).
- [46] Y. Liu, D. B. Haviland, B. Nease, and A. M. Goldman, *Phys. Rev. B* **47**, 5931 (1993).
- [47] Y. Ivry, C.-S. Kim, A. E. Dane, D. De Fazio, A. N. McCaughan, K. A. Sunter, Q. Zhao, and K. K. Berggren, *Phys. Rev. B* **90**, 214515 (2014).
- [48] W. Zhao, Q. Wang, M. Liu, W. Zhang, Y. Wang, M. Chen, Y. Guo, K. He, X. Chen, Y. Wang *et al.*, *Solid State Commun.* **165**, 59 (2013).
- [49] M. S. M. Minhaj, S. Meepagala, J. T. Chen, and L. E. Wenger, *Phys. Rev. B* **49**, 15235 (1994).